Computer Methods and Programs in Biomedicine 184 (2020) 105120

Contents lists available at ScienceDirect

Computer Methods and Programs in Biomedicine

journal homepage: www.elsevier.com/locate/cmpb

Automated detection and localization system of myocardial infarction in single-beat ECG using Dual-Q TQWT and wavelet packet tensor decomposition

Jia Liu[a,b], Chi Zhang[a], Yongjie Zhu[a,b], Tapani Ristaniemi[b], Tiina Parviainen[c], Fengyu Cong[a,b,*]

[a] School of Biomedical Engineering, Faculty of Electronic Information and Electrical Engineering, Dalian University of Technology, Dalian, China
[b] Faculty of Information Technology, University of Jyvaskyla, Jyvaskyla, 40014, Finland
[c] Centre for Interdisciplinary Brain Research, Department of Psychology, Faculty of Education and Psychology, University of Jyvaskyla, Jyvaskyla, 40014, Finland

ARTICLE INFO

Article history:
Received 13 August 2019
Revised 3 October 2019
Accepted 3 October 2019

Keywords:
Electrocardiogram (ECG)
Myocardial infarction (MI)
Dual-Q tunable Q-factor wavelet transformation (Dual-Q TQWT)
Discrete wavelet packet transform (DWPT)
Multilinear principal component analysis (MPCA)

ABSTRACT

Background and objective: It is challenging to conduct real-time identification of myocardial infarction (MI) due to artifact corruption and high dimensionality of multi-lead electrocardiogram (ECG). In the present study, we proposed an automated single-beat MI detection and localization system using dual-Q tunable Q-factor wavelet transformation (Dual-Q TQWT) denoising algorithm.
Methods: After denoising and segmentation of ECG, a fourth-order wavelet tensor (leads × subbands × samples × beats) was constructed based on the discrete wavelet packet transform (DWPT), to represent the features considering the information of inter-beat, intra-beat, inter-frequency, and inter-lead. To reduce the tensor dimension and preserve the intrinsic information, the multilinear principal component analysis (MPCA) was employed. Afterward, 84 discriminate features were fed into a classifier of bootstrap-aggregated decision trees (Treebagger). A total of 78 healthy and 328 MI (6 types) records including 57557 beats were chosen from PTB diagnostic ECG database for evaluation.
Results: The validation results demonstrated that our proposed MI detection and localization system embedded with Dual-Q TQWT and wavelet packet tensor decomposition outperformed commonly used discrete wavelet transform (DWT), empirical mode decomposition (EMD) denoising methods and vector-based PCA method. With the Treebagger classifier, we obtained an accuracy of 99.98% in beat level and an accuracy of 97.46% in record level training/testing for MI detection. We also achieved an accuracy of 99.87% in beat level and an accuracy of 90.39% in record level for MI localization.
Conclusion: Altogether, the automated system brings potential improvement in automated detection and localization of MI in clinical practice.

1. Introduction

Myocardial infarction (MI) is defined as myocardial cell death due to prolonged ischemia [1]. As one of the main causes of death and disability, MI is an intractable disease and can result in artery disease. In clinical practice, many techniques, including electrocardiographic (ECG), biochemical markers, imaging and so on, are used to assist in the diagnosis of MI. Among these techniques, the non-invasive ECG, an economic tool, is widely used in MI detection [2,3]. The ECG abnormalities of MI can be observed in the PR segment, the QRS complex, the ST segment or the T wave [1]. However, the diagnosis of MI usually requires multiple ECGs because the ECG signals are time-varying in nature with small amplitude. Manual inspection in clinical practice is not only time-consuming and strenuous but also leads to inter- and intra-evaluator variability [4,5]. Therefore, a computer-aided diagnosis system (CADS) of MI should be developed to realize time-saving and reliable analysis [6–11].

Good quality ECG is a guarantee of reliable CADS, while the ECG signals are often corrupted by noise [12]. The ECG signals are usually mixed with different kinds of artifacts, such as power line interference, muscle artifacts, and baseline drifts. Therefore, it is necessary to remove artifacts by implanting denoising method in CADS. In [13], Fatin and colleagues removed the low frequency 0–0.351 Hz and high frequency >45 Hz from ECG with 6-level

* Corresponding author at: School of Biomedical Engineering, Dalian University of Technology, Dalian, China.
E-mail addresses: jialiu15@foxmail.com (J. Liu), cong@dlut.edu.cn (F. Cong).

https://doi.org/10.1016/j.cmpb.2019.105120
0169-2607/

db6 discrete wavelet transform (DWT) decomposition in arrhythmia recognition. However, the DWT fails to separate the noise from ECG when two types of signals co-occur at the same frequency band. According to the nature of waveforms in ECG, the morphological-based algorithm should be considered in ECG denoising. Blanco-Velasco et al. [14] applied the empirical mode decomposition (EMD), in which partial intrinsic mode functions (IMFs) were reconstructed to remove noise mixed with ECG from the MIT-BIH database. Although EMD has been widely used in ECG denoising, it still leads to the mode-mixing problem [15]. Therefore, it is challenging to find an effective denoising method to obtain high signal-noise-ratio (SNR) ECG signal. Dual-Q tunable Q-factor wavelet transformation (Dual-Q TQWT), a morphological-based algorithm, was first introduced in [16–18]. Although Dual-Q TQWT is applied to speech analysis [16], limited attention has been focused on ECG denoising until now. Using the resonance-based morphological separation, the Dual-Q TQWT might provide new sight for ECG denoising. In our study, we applied the Dual-Q TQWT as a denoising method in MI detection and localization system.

Feature extraction plays an important role in CADS. Recent studies have developed effective feature extraction methods in automated MI detection and localization system, as shown in Table 5. In [10], a multiscale energy and eigenspace approach was proposed based on DWT. The approach obtained an accuracy of 99.58% in MI localization with 72 features from frame-based (4 beats) ECG. Sun et al. [7] presented a multiple instance learning for MI detection system based on time-domain features of ST segments and R-R intervals from ECG. Their method obtained a sensitivity of 92.6% in single-beat MI detection with 74 features. Similarly, 36 time-domain features of Q wave, T wave, and ST level elevation were extracted in [3]. They achieved an accuracy of 98.3% in single-beat MI detection. In addition to linear time-domain features, Acharya et al. [11] calculated 12 types of nonlinear features covering different types of entropy, fractal dimension, and Lyapunov exponent. They obtained an accuracy of 98.8% in MI detection with 47 features based on single-beat and single-lead ECG. However, it is still challenging to propose efficient and low complexity feature extraction approaches to extract discriminate and generalization features. The tensor decomposition, different from other state-of-art feature extraction methods, can directly exploit multi-mode information contained in the tensor structure. Using tensor decomposition, the information of inter-lead, inter-beat, intra-beat, and inter-frequency can be considered as parameters. Especially, considering the lead of ECG as a parameter instead of manual selection can avoid under-fitting (single-lead) or over-fitting (12-lead). Sibasankar et al. [8] developed a third-order tensor method (leads × beats × samples) for MI detection and localization, but they failed to achieve high performance in single-beat ECG based on DWT. In their study, they selected discriminant features from different tensor modes in different wavelet coefficients of DWT with visual observation, impeding the precise frequency and automated data-driven analysis. In contrast, the discrete wavelet packet transform (DWPT) has these advantages: each layer has an equal number of wavelet packet coefficients; the last layer can cover all the frequency subbands. These advantages provide the possibility of fourth-order tensor formation.

In our present study, we presented an automated MI detection and localization system equipped with Dual-Q TQWT denoising method and fourth-order wavelet packet tensor (leads × subbands × samples × beats). The tensor-based MPCA was applied to reduce the dimensionality of the wavelet packet tensor. The optimal features were classified by a classifier of bootstrap-aggregated decision trees (Treebagger). In our system, the MI detection, a two-class classifier, is used to distinguish MI patients from healthy volunteers for preliminary screening. The MI localization, a multi-class classifier, is a progressive diagnosis for different types of MI patients. The two-step MI classification is precise and resource efficient in practice. The PTB diagnostic ECG database was chosen for system evaluation.

Table 1
Numbers of records and beats from different groups.

Type	AMI	ALMI	IMI	ASMI	ILMI	IPLMI	H
Records	46	42	89	76	56	19	78
Beats	6306	6568	12,115	11,232	8280	2714	10,342

2. Database

The ECG signals were chosen from the Physikalisch-Technische Bundesanstalt (PTB) [19] diagnostic ECG database provided by PhysioBank [20]. A total of 549 records from 290 subjects (mean age = 57.2 years, 209 men) were collected in the Department of Cardiology of University Clinic Benjamin Franklin in Berlin, Germany. Each record contains 12 conventional leads (I, II, III, AVR, AVL, AVF, V1, V2, V3, V4, V5, V6) and 3 Frank leads (VX, VY, VZ) ECG, which were digitized at 1000 Hz with 16 bit resolution over a range of ±16.384 mV. According to the clinical statistics, 268 subjects' data, including eight different heart disease groups (216) and one healthy group (52), were provided in the database. Among these groups, the myocardial infarction group diagnosed as six different MIs (anterior: AMI, anterior-lateral: ALMI, inferior: IMI, anterior-septal: ASMI, inferior-lateral: ILMI, inferior-posterior-lateral: IPLMI) and the healthy group (H) were chosen for MI detection and localization evaluation in the present study. The numbers of records and beats from MI patients and healthy volunteers were listed in Table 1.

3. Methods

The present study presented a novel MI detection and localization system using Dual-Q TQWT denoising method and wavelet packet tensor decomposition. The diagram of detection and localization system is shown in Fig. 1. For the preprocessing stage, ECG data were down-sampled to 250 Hz and filtered with 1000-order 0.5 Hz high-pass and 40 Hz low-pass FIR filters implanted in EEGLAB [21]. Furthermore, a mean value was subtracted from each lead to eliminate the offset effect [22]. The Dual-Q TQWT, apart from the conventional methods, was applied to ECG denoising.

3.1. Denoising with Dual-Q TQWT

The Dual-Q TQWT is a resonance-based, rather than a frequency or scale based signal decomposition algorithm, which utilizes sparse signal representations and morphological component analysis (MCA) [18]. Using this method, a signal can be decomposed into the sum of a high-resonance component and a low-resonance component. Each component is represented sparsely by TQWT algorithm with high Q-factor and low Q-factor.

TQWT is a discrete wavelet transform with flexible Q-factor [17]. Three parameters: Q-factor (Q), the redundancy (r), and decomposition level (J) should be set during TWQT decomposition. The frequency responses and wavelets of different parameters are displayed in Fig. 2. The parameter Q is related to oscillation numbers of wavelet, and the parameter r is an index of the overlapping between adjacent frequency responses. All three parameters are closely related. TQWT is developed as J level of two-channel filter banks attaching to low-pass filter output, resulting in $J+1$ subbands. The low- pass ($H_0^{(j)}(w)$) and high-pass ($H_1^{(j)}(w)$) filters

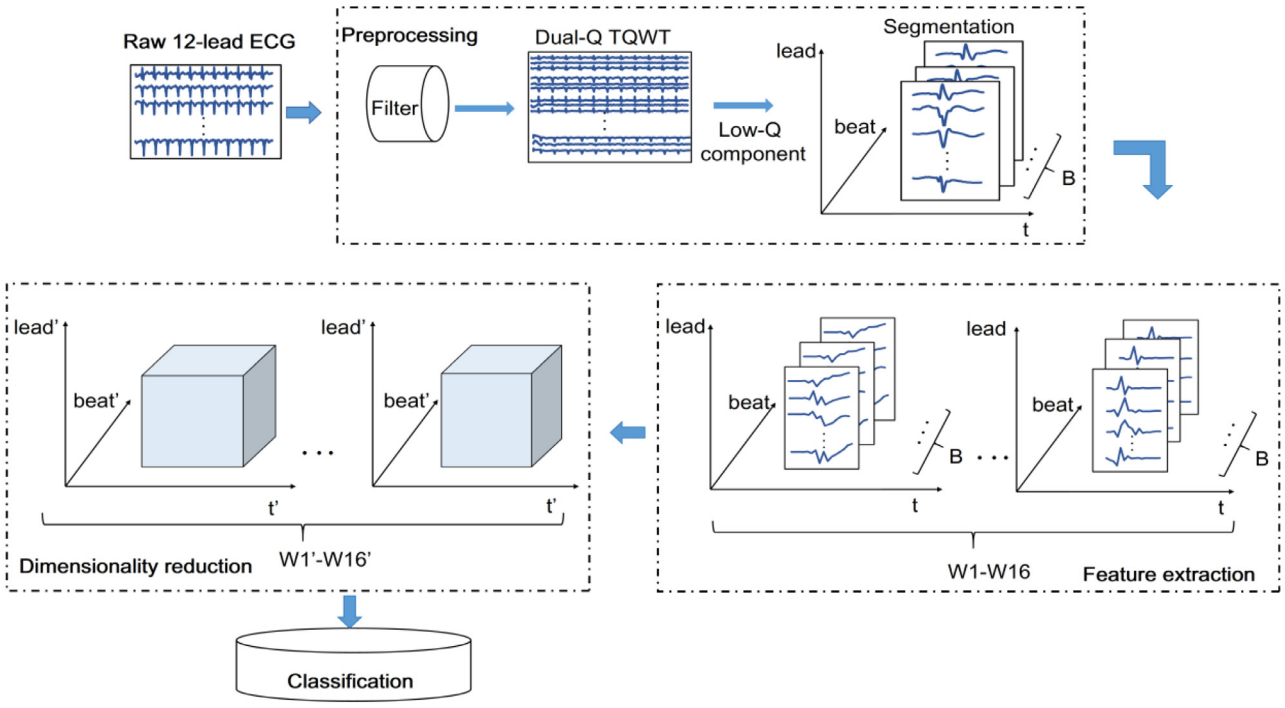

Fig. 1. Schematic diagram of MI detection and localization system.

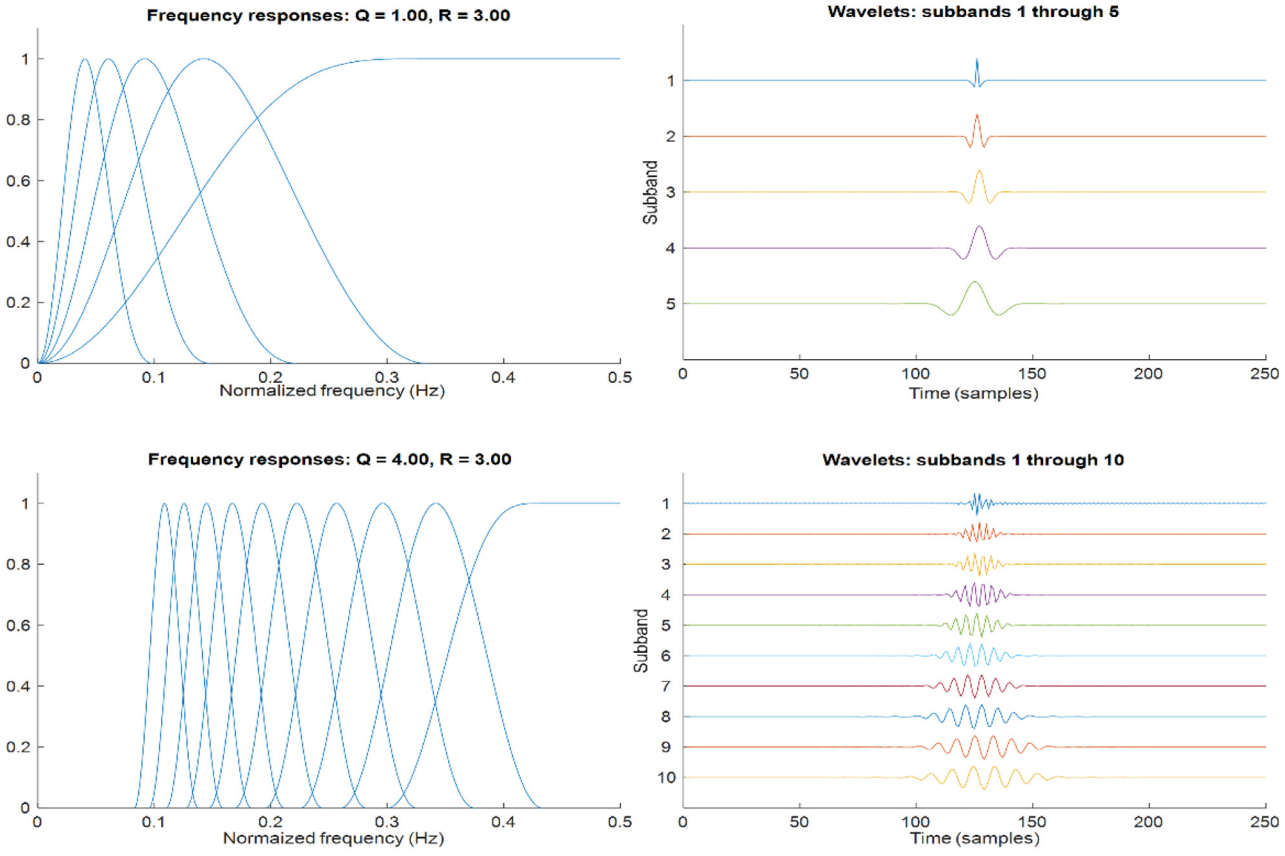

Fig. 2. Frequency responses and wavelets of TQWT with $Q=1$, $J=4$ (top) and $Q=4$, $J=9$ (down).

are defined as:

$$H_0^{(j)}(w) = \begin{cases} \prod_{m=0}^{j-1} H_0\left(\frac{w}{\alpha^m}\right), & |w| \le \alpha^j \pi \\ 0, & \alpha^j \pi < |w| \le \pi \end{cases} \quad (1)$$

$$H_1^{(j)}(w) = \begin{cases} H_1\left(\frac{w}{\alpha^{j-1}}\right) \prod_{m=0}^{j-2} H_0^j\left(\frac{w}{\alpha^m}\right), & (1-\beta)\alpha^{j-1}\pi \le |w| \le \alpha^{j-1}\pi \\ 0, & for\ others\ w \in [-\pi\ \pi] \end{cases} \quad (2)$$

where low-pass scaling $\alpha \le 1$, and high-pass scaling $\beta \le 1$. The parameters Q and r are given by:

$$r = \frac{\beta}{1-\alpha} \quad (3)$$

$$Q = \frac{f_c}{BW} = \frac{2-\beta}{\beta} \quad (4)$$

where BW and f_c are the bandwidth and center frequency, respectively.

Given a signal $\mathbf{x}$, Dual-Q TQWT decomposes $\mathbf{x}$ into $\mathbf{x_1}$ and $\mathbf{x_2}$ components, where $\mathbf{x_1}$ consists largely of oscillations and $\mathbf{x_2}$ consists largely of transients. The $\mathbf{x}$ is the sum of $\mathbf{x_1}$ and $\mathbf{x_2}$. Using TQWT, x can be denoted as $TQWT_1$ and $TQWT_2$ with high and low Q-factors. The constrained optimization problem can be represented as [16]:

$$argmin_{\boldsymbol{w}_1, \boldsymbol{w}_2} \sum_{j=1}^{J1+1} \lambda_{1,j} \left\| \boldsymbol{w}_{1,j} \right\|_1 + \sum_{j=1}^{J2+1} \lambda_{2,j} \left\| \boldsymbol{w}_{2,j} \right\|_1 \quad (5)$$

$$\mathbf{x} = \mathbf{x}_1 + \mathbf{x}_2 = \mathrm{TQWT}_1{}^{-1}(\boldsymbol{w}_1) + \mathrm{TQWT}_2{}^{-1}(\boldsymbol{w}_2) \quad (6)$$

where $\boldsymbol{w}_{i,j}$ denotes subband j of $TQWT_i$ for $i = 1,2$. The λ_1 and λ_2, computed from the norms of wavelets based on the mentioned three parameters in TQWT, are the regularization parameters for high and low Q-factor TQWT. The MCA [23] based on split augmented Lagrangian shrinkage algorithm (SALSA) [24] is applied to estimate the solution of the optimization problem. The six parameters, Q_1, r_1, J_1 for high Q-factor TQWT and Q_2, r_2, J_2 for low Q-factor TQWT, should be preset considering the mathematical theory of TQWT, ECG morphology, running time, and goodness-of-fit. To prevent an excessive ringing of wavelets, the parameter r should be set as greater than or equal to 3 [9,25]. In our study, the parameters r_1 and r_2 are equal to 3, consistent with literature studies [25,26]. The low factor Q_2 is usually set to 1 [16], while the high factor Q_1 is set to 4 in our work. The parameters J is set as half of the maximum of $J_{\max}$ with $J_1 = 10$, $J_2 = 25$ because low J cannot cover the signal and high J leads to high dimension computations [27–29].

$$J_{max} = \left\lfloor \frac{\log(\beta N - 8)}{log(1-\alpha)} \right\rfloor \quad (7)$$

where N is the number of samples of ECG signal.

After filtering and denoising, the ECG signals were segmented into beats based on R-peak, detected by the Pan-Tompkins algorithm [30]. Each beat has 162 samples including 250 ms before and 400 ms after R-peak detection. A total of 57,557 ECG beats were obtained from 6 types of MI groups and 1 healthy group, as shown in Table 1.

3.2. Feature extraction by DWPT

The discrete wavelet packet transform (DWPT) has been successfully used in ECG feature extraction [31]. Compared with the DWT, the DWPT provides more spectral information in detail. Let $\mathbf{S} = [\mathbf{s}_1, \mathbf{s}_2, \ldots, \mathbf{s}_v]$ be a 12-lead ECG beat of one subject, where $v = 12$ leads, $Ls = 162$ samples, $S \in R^{Ls \times v}$. In the DWPT, both the approximation and detail coefficients are decomposed in each level, resulting in 2^J subbands at J^{th} level decomposition. The sample length of the sub-band at j level is ls, where $ls \cong Ls/2^j$. In our study, the preprocessed ECG beats were subjected to 4 levels of DWPT using db4 mother wavelet to extract concise and distinctive features. We chose 16 subbands at the 4th decomposition level covering all the frequency bands, each of which contained specific characteristics. The 16 subbands have the same number of coefficients (16 samples), which provides good feasibility for wavelet packet tensor decomposition analysis. The wavelet packet coefficient matrix extracted from 12-lead m^{th} beat is converted into wavelet packet tensor $\mathcal{W}_m \in \boldsymbol{R}^{I_1 \times I_2 \times I_3}$, where the modes of I_1, I_2, I_3 are the 12-lead of ECG, the 16 subbands of DWPT at 4th level, and the 16 samples of each subband. Hence, a total of B wavelet packet tensors from all subjects are represented as $\mathcal{W} = [\mathcal{W}_1, \mathcal{W}_2, \ldots, \mathcal{W}_m, \ldots, \mathcal{W}_B]$, where $m = 1, 2, \ldots, B$.

3.3. Dimensionality reduction by MPCA

In the view of the high dimensionality of wavelet packet tensor, it is necessary to reduce the dimensionality of discriminate features to obtain a good performance of pattern recognition and to improve processing speed with less memory capacity. Compared with vector-based dimensionality reduction algorithm of principal component analysis (PCA), the multilinear principal component analysis (MPCA) can be applied to a tensor object for feature extraction and dimensionality reduction [32,33]. Although MPCA is widely used in other fields, such as gait recognition [32] and face recognition [34], the application in multivariate time series has not been promoted [31,35].

The MPCA is realized following 4 steps [32]. First, the data are preprocessd by centralizing the input samples. Second, data are initialized by calculating the eigen-decomposition of the eigenvectors corresponding to the most significant eigenvalues. The input of MPCA are wavelet packet tensors of B beats, $\in \boldsymbol{R}^{I_1 \times I_2 \times I_3 \times B}$. Using a multilinear transformation $\{\tilde{\mathbf{U}}^{(n)} \in \mathrm{R}^{I_n \times I_n'},\ I_n' \le I_n,\ n = 1, 2, \ldots, N,\ N = 3\}$, where the $\tilde{\mathbf{U}}^{(n)}$ is the n^{th} projection matrix, the input tensor $\boldsymbol{R}^{I_1 \times I_2 \times I_3}$ of each beat $\mathcal{W}_m$ can be mapped onto a low dimensionality tensor space $\boldsymbol{R}^{I_1' \times I_2' \times I_3'}$ to extract optimal features. The low dimensionality output of MPCA with maximum captured variation is represented as:

$$\mathcal{Y}_m = \mathcal{W}_m \times \tilde{\mathbf{U}}^{(1)^T} \times_2 \tilde{\mathbf{U}}^{(2)^T} \times_3 \tilde{\mathbf{U}}^{(3)^T} \quad (8)$$

where $\mathcal{Y}_m \in \boldsymbol{R}^{I_1' \times I_2' \times I_3'}$, B beats of outputs are $\mathcal{Y} = [\mathcal{Y}_1, \mathcal{Y}_2, \ldots, \mathcal{Y}_m, \ldots, \mathcal{Y}_B]$, $\mathcal{Y} \in \boldsymbol{R}^{I_1' \times I_2' \times I_3' \times B}$. The realization of dimension reduction can be simplified as an optimal problem:

$$\left\{\tilde{\mathbf{U}}^{(n)^T},\ n = 1,\ 2,\ 3\right\} = argmax_{\tilde{\mathbf{U}}^{(1)},\ \tilde{\mathbf{U}}^{(2)},\ \tilde{\mathbf{U}}^{(3)}}\ \psi_{\mathcal{Y}} \quad (9)$$

where $\psi_{\mathcal{Y}}$ is the total of B transformed tensor scatters, and $\psi_{\mathcal{Y}} = \sum_{m=1}^{B} \|\mathcal{Y}_m - \bar{\mathcal{Y}}\|_F^2$, where the $\bar{\mathcal{Y}} = (\sum_{m=1}^{B} \mathcal{Y}_m)/B$. Based on the solution of Eq. (8), the scatter of n-mode unfolding matrix is given by:

$$\boldsymbol{\Phi}^{(n)} = \sum\nolimits_{m=1}^{B} \left(\mathbf{W}_m^{(n)} - \bar{\mathbf{W}}_m^{(n)}\right) \cdot \tilde{\mathbf{U}}_{\Phi(n)} \cdot \tilde{\mathbf{U}}^T{}_{\Phi(n)} (\mathbf{W}_m^{(n)} - \bar{\mathbf{W}}_m^{(n)})^T \quad (10)$$

Where $\mathbf{W}_m^{(n)}$ is the n-mode unfolding matrix of the tensor $\mathcal{W}_m$, and $\tilde{\mathbf{U}}_{\Phi(n)}$ can be evaluated as:

$$\tilde{\mathbf{U}}_{\Phi(n)} = \tilde{\mathbf{U}}^{(n+1)} \otimes \tilde{\mathbf{U}}^{(n+2)} \otimes \ldots \otimes \tilde{\mathbf{U}}^{(N)} \otimes \tilde{\mathbf{U}}^{(1)} \otimes \tilde{\mathbf{U}}^{(2)} \ldots \otimes \tilde{\mathbf{U}}^{(n-1)} \quad (11)$$

where $\otimes$ is the Kronecker product. The optimization step is solved using the Eqs. (10) and (8) in the iteration. Finally, the high-dimensional data are projected into low-dimensionality tensor space.

3.4. Classification

The optimal features extracted from MPCA were fed into a classifier. As a decision support tool, the decision tree (DT) utilizes a tree-like model of decisions and possible consequences. It is a directed graph, with three sets of decision, chance, and terminal nodes (also known as leaves) [36]. A DT, equipped with two functions of denoting payoffs and probabilities, can be learned in a recursive partitioning manner based on an attribute value test. Although DT has an advantage of simplicity, it is unstable and easily affected by noise. The Bootstrap-aggregated, one of the most popular techniques for constructing ensembles to improve the robustness, takes base DT learner and invokes it many times with replacement samples [37]. As an important parameter of Treebagger, the number of trees can reach several hundreds or thousands depending on the nature of the training sets. By taking the majority votes or averaging predictions of different DTs, the Treebagger leads to better performance than a DT.

In our study, the performance of classifiers was measured by sensitivity (SE), specificity (SP), and accuracy (ACC) [38]. Based on the confusion matrix obtained from predicted class and actual class, the SE, SP, and ACC are evaluated as:

$$\mathrm{SE} = \frac{\mathrm{TP}}{\mathrm{TP} + \mathrm{FN}} \tag{12}$$

$$\mathrm{SP} = \frac{\mathrm{TN}}{\mathrm{TN} + \mathrm{FP}} \tag{13}$$

$$\mathrm{ACC} = \frac{\mathrm{TP} + \mathrm{TN}}{\mathrm{TP} + \mathrm{TN} + \mathrm{FP} + \mathrm{FN}} \tag{14}$$

where TP, TN, FP, and FN correspond to true positive, true negative, false positive, and false negative. The ROC (receiver operating characteristics) was also adopted to visualize the performance of classifiers [39].

4. Results and discussion

Using 78 healthy and 328 MI records chosen from the PTB ECG database, the novel detection and localization system of MI with Dual-Q TQWT and wavelet packet tensor decomposition proposed in our work were evaluated. First, we evaluated the performance of these algorithms in our system. According to the good performance of the algorithms, we distinguished the MI patients from healthy volunteers with single-beat ECG. Furthermore, each specific MI patient was localized at one of 6 different MI types. Finally, our automated MI detection and localization system was compared with earlier published studies.

4.1. ECG denoising and MPCA evaluation

Based on high and low Q-factors wavelets and frequency responses, as shown in Fig. 2, Dual-Q TQWT decomposes the filtered ECG signal into the sum of a high Q-factor component and a low Q-factor component. Fig. 3 displays the decomposition results consisting of original and resonance waveforms. From this figure, we found that the high Q-factor component corresponded to sustained oscillations, consisting of low- and high-frequency bands unrelated to typical morphology of ECG (e.g. PR segment, QRS waveform, et al.). In contrast, the low Q-factor component corresponded to the transients following the morphology of the original waveform, with high signal-noise-ratio (SNR). Due to the characteristics of morphological segments and high SNR, the low Q-factor component was chosen for further processing. The denoised data were segmented into beats and decomposed into 4-level DWPT to extract features. Using 16 subbands in the fourth level, a wavelet packet tensor (leads × subbands × samples × beats) was formed. In our work, the MPCA was applied to wavelet packet tensor for dimensionality reduction. Compared with the vector-based PCA, the tensor-based MPCA could reserve inherent properties of features.

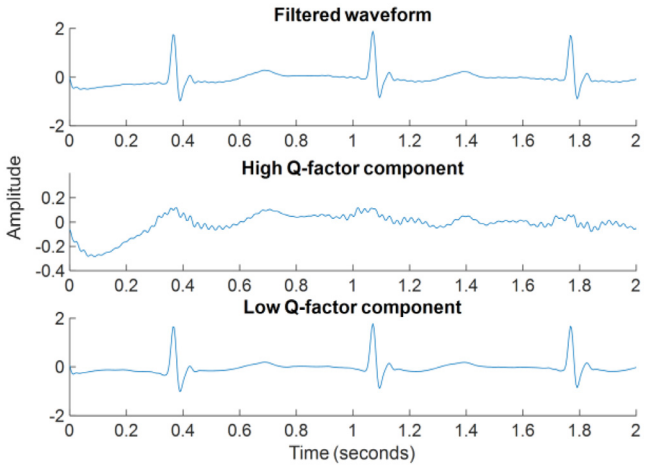

Fig. 3. Resonance decomposition with Dual-Q TQWT.

Table 2
Comparisons among denoising methods.

	Filtered	Dual-Q TQWT	DWT	EMD
ACC	83.64%	91.36%	89.89%	91.28%
SEN	96.73%	98.27%	97.98%	98.26%
SPE	83.74%	91.36%	89.89%	91.27%
Time(s)	-	45.63	2.98	225.89

To illustrate the performance of the denoising algorithm, we compared the Dual-Q TQWT with commonly used denoising methods discrete wavelet transform (DWT) [13] and empirical mode decomposition (EMD) [13]. Based on the data from healthy volunteers and 5 groups of MI (without IPLMI), the performance of a multi-class classifier of Treebagger in the record level was chosen as criteria of these comparisons. The comparison results are illustrated in Table 2. The results demonstrate that the performance of denoising methods outperforms filter processing. Compared with the state-of-art denoising methods (DWT and EMD), our proposed Dual-Q TQWT is comparable considering the running time (s/record) and performance. The good results validate the utility of Dual-Q TQWT denoising in MI detection and localization system.

For wavelet packet coefficients, we compared the results of WPT-Tensor and WPT-Vector (by reshaping wavelet packet tensor to vector). WPT-Vector achieved an accuracy, a sensitivity, and a specificity of 88.73%, 97.75%, and 88.75%, respectively. We also computed the performance of Dual-Q TQWT time-domain features without DWPT and obtained an accuracy, a sensitivity, and a specificity of 81.24%, 91.56%, and 80.95%, respectively. Altogether, the combination of Dual-Q TQWT + DWPT + MPCA yielded the highest performance compared with Dual-Q TQWT + DWPT + PCA and Dual-Q TQWT + MPCA.

4.2. Physiological ECG features from DWPT and MPCA

By applying DWPT, we extracted spatial, spectral, and temporal features from leads, frequency bands (subbands), and samples. Fig. 4 displays the physiological ECG waveforms in subbands 1–4 (significant variation of features) from 12 leads. We found that the waveforms in different subbands and leads were different in 6 types of MI patients and healthy volunteers. The abnormalities of MI could be displayed in the PR segment, the QRS complex, the ST segment, and the T wave in different subbands.

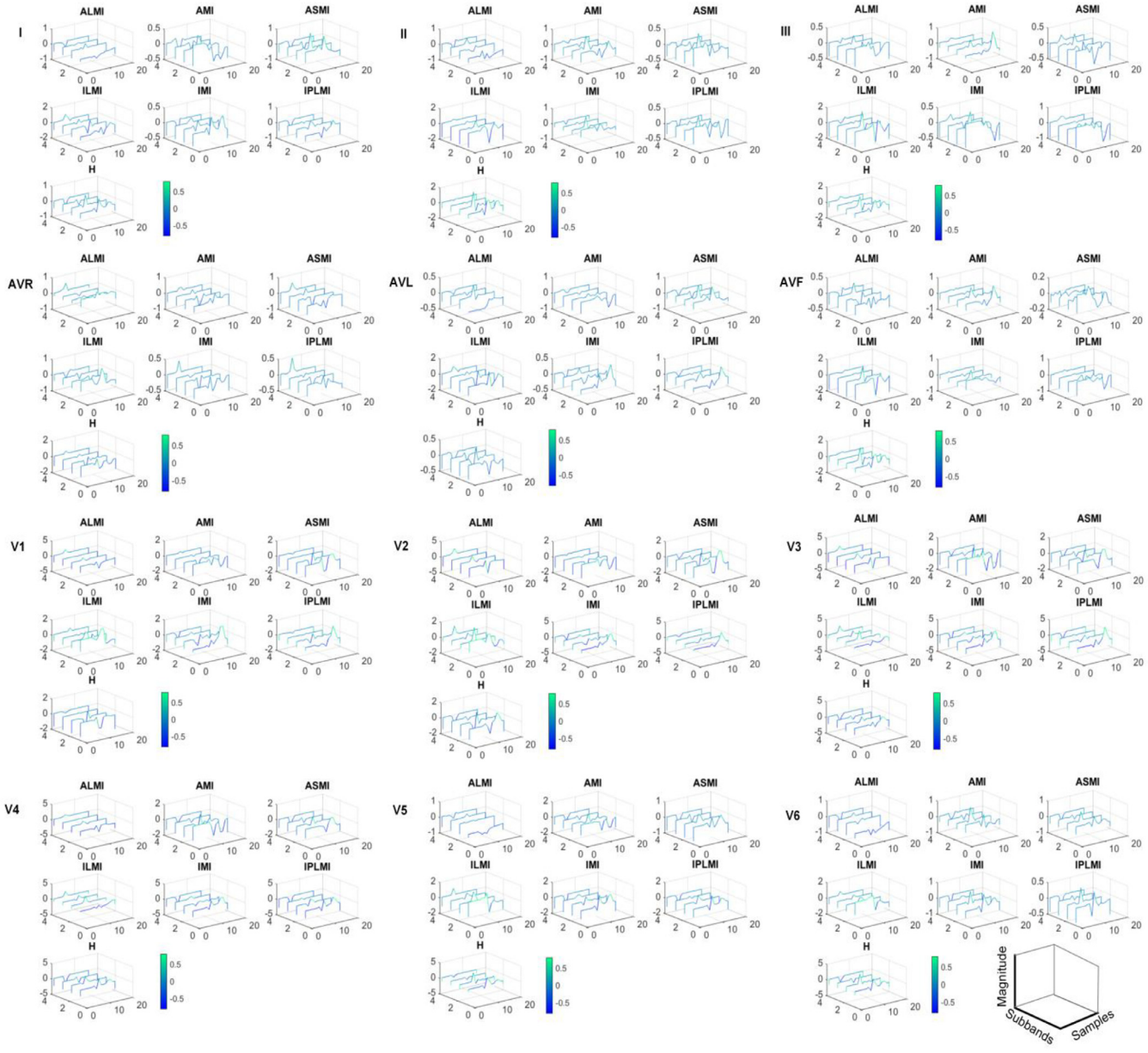

Fig. 4. DWPT features extracted from leads, sunbands, and samples of MI patients and healthy volunteers.

Although DWPT features are significantly different in different types of MI and healthy volunteers, as shown in Fig. 4, there is too much redundancy information in the fourth-order wavelet packet tensor. The wavelet packet tensor was subjected to MPCA and was reduced to low-dimensional tensor using matrices of multilinear projection. Fig. 5 displays three projection matrices in three modes. According to multilinear projection, we found four components in the spatial factor, which illustrated the multilinear combination of 12 leads. For the spectral factor, we found three components, especially subbands 1, 2, and 4, which were most important in MI identification. Each subband covers about 8 Hz from 0.5–125 Hz. Seven waveforms in the temporal factor were the representations of the PR segment, the QRS complex, the ST segment, and the T wave. The discriminant features of different types of MI patients and healthy volunteers are located in 4 components of spatial factor, 3 components of spectral factor, and 7 components of temporal factor.

4.3. MI detection

The MI detection was treated as a two-class classification, distinguishing the MI patients from healthy volunteers. There were 47,215 instances (heart beats) from 328 MI records and 10,342 instances from 78 healthy records. The dimensions (12 leads $\times$ 16 subbands $\times$ 16 samples $\times$ 57,557 beats) of wavelet packet tensor were reduced to low-dimension space of $4 \times 3 \times 7 \times 57{,}557$ beats by MPCA, where 90% energy was kept and the maximum number of interaction was set as 1. A total of 84 maximum optimal features were selected for MI detection. A Treebagger embedded with 200 trees was applied to classification. Fig. 6 shows the ROC curves corresponding to different sets of features (according to the ordering index of projected features in decreasing variance) with 90% instances for training and 10% for testing, which demonstrates the 84 features are not overfitting or underfitting.

We conducted training processes in both beat level (randomly selected instances from records) with 10-fold cross validation and

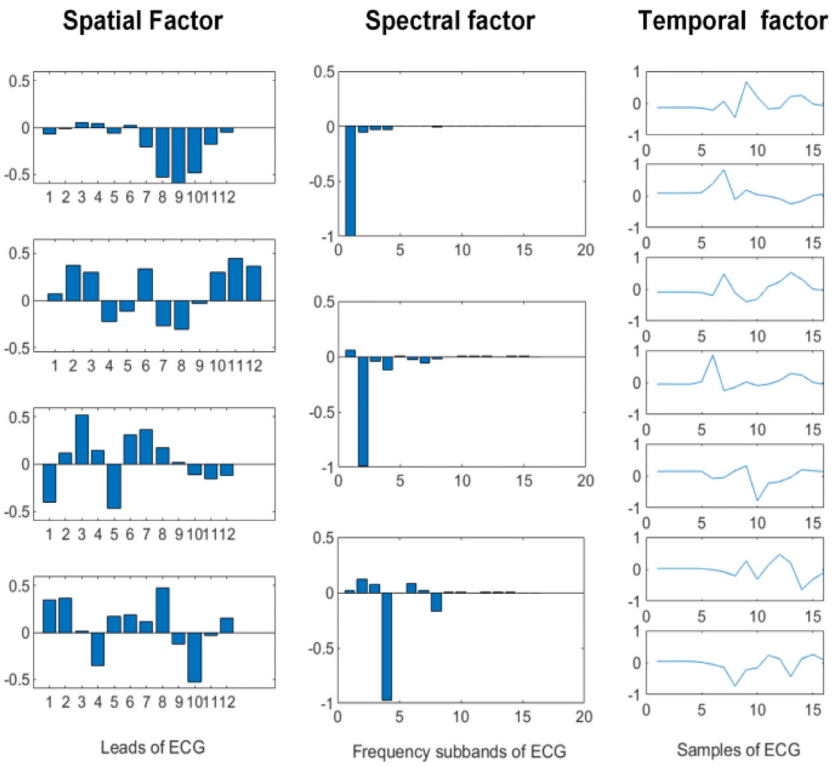

Fig. 5. MPCA matrices of multilinear projection.

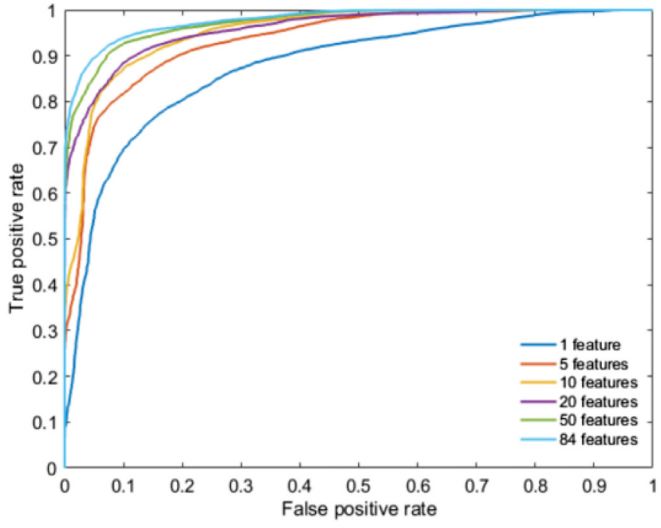

Fig. 6. ROC for MI detection with different features.

record level (considered instances from a set of MI and healthy records to avoid the same instance during training and testing) with handout method. For the training in beat level, we achieved an accuracy of 99.98%, a sensitivity of 100%, and a specificity of 99.90%, respectively. The confusion matrix of MI detection is shown in Table 3. As shown in the table, all 18,852 MI beats could be correctly classified, while 8 healthy beats of ECG among 4106 beats were misclassified to MI patients. Using only 10 features, we could achieve an accuracy of 99.41% for MI detection. For the training in record level, we selected randomly 90% records for training and the left 10% records for testing. We achieved an accuracy of 97.46%, a sensitivity of 99.09%, and a specificity of 90.26%, respectively. Compared with beat level classification results, the record level results reveal the inter-record and inter-subject variations.

Table 3
Confusion matrix of Treebagger for MI detection.

	H	MI
H	4162	8
MI	0	18,852

4.4. MI localization

In this section, the MI localization was seen as multi-class classification, localizing each specific group from 6 different types of MI. The 47,215 MI instances came from 46 AMI (6306), 42 ALMI (6568), 89 IMI (12,115), 76 ASMI (11,232), 56 ILMI (8280), and 19 IPLMI (2714) records. The dimensions (12 leads $\times$ 16 subbands $\times$ 16 samples $\times$ 47,215 beats) of wavelet packet tensor were reduced to low-dimension $4 \times 3 \times 7 \times 47{,}215$ beats by MPCA with the same settings in MI detection. The same classifier and beat- and record-level training processes were chosen for MI localization. Fig. 7 displays the changes in average accuracy, sensitivity, and specificity following the number of features with 10-fold cross validation, which demonstrates the necessity of 84 features in MI localization. For the beat level, the average accuracy, sensitivity, and specificity were 99.87% ($\pm$ 0.05%), 99.97% ($\pm$ 0.01%), and 99.88% ($\pm$ 0.05%), respectively. The confusion matrix of 6 types of MI is presented in Table 4. From the confusion matrix, we found that all the ILMI beats could be classified correctly. Other types of MI were easily misclassified into IPLMI, with 5 AMI beats, 2 ALMI beats, 3 IMI beats, and 3 ASMI beats. The beats of ASMI were easily mixed with other types of MI. By using only 10 features, we could achieve an accuracy of 99.35% for MI localization. For the record level, we presented the performance with 90% records for training and the left 10% records for testing. We achieved an accuracy of 90.39%, a sensitivity of 98.03%, and a specificity of 90.76%, respectively.

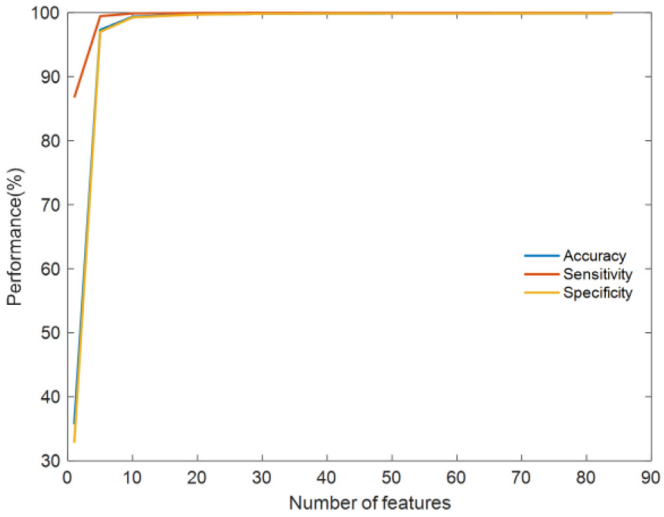

Fig. 7. Performance of MI localization with different features using 10-fold cross validation.

Table 4
Confusion matrix of Treebagger for MI localization.

	AMI	ALMI	IMI	ASMI	ILMI	IPLMI
AMI	2576	2	0	1	0	5
ALMI	2	2502	2	2	0	2
IMI	1	1	4563	3	0	3
ASMI	2	0	2	4798	0	3
ILMI	0	0	0	0	1115	0
IPLMI	0	0	2	1	0	3298

4.5. Comparison performance

Table 5 summarizes the studies employing different techniques in MI detection and localization with the same PTB ECG dataset. In our study, we down-sampled the ECG signal from 1000 Hz to 250 Hz, resulting in 162 samples in each beat. The samples in each beat are fewer than 650 samples in previous research [6,9,31]. Furthermore, a denoising method was applied differently from previous conventional filtering preprocessing. In comparison to filtered data and commonly used denoising methods, the advent of Dual-Q TQWT makes it possible to obtain better performance with fewer samples in each beat. To enhance real-time MI diagnosis, our work, as well as some earlier studies [8,10], was focused on single-beat rather than frame-based (4 beats) exploration. Furthermore, the number of ECG leads is another factor correlated with diagnosis efficiency and computer capacity. Instead of considering all 12 leads, some researchers explored the possibility of using fewer leads or just one single lead [6,9,11,40]. However, they only illustrated the single lead or 12 leads, ignoring the combination of different leads. Wavelet packet tensor is an efficient tool, which can take the ECG leads as one part of features. Using dimensionality reduction, optimal leads are selected, avoiding a manual operation of over-fitting or under-fitting. Different from third-order tensor used in [8], our work applied a fourth-order tensor consisting of frequency (taking advantage of an equal number of wavelet packet coefficients), leads, samples, and beats. The fourth-order wavelet packet tensor was dimensionality reduced in the tensor structure with MPCA, whose classification performance outperformed the commonly used vector-based PCA. Although feature extraction and selection were eliminated in these studies with convention neural network (CNN) [6,40–43], big data, long training time, and high quality service were other problems introduced in their studies. Previous studies achieved good performance without considering inter-subjects variations. Our study presented good results in both beat level and record level training/testing. The MI detection and localization system for single-beat containing fewer samples in our

Table 5
Comparison of studies using PTB ECG database.

Ref	Beat	Lead	Database	Over-fitting	Methods	Features	Results
[6]	1	12	MI: 369 RE H: 79 RE	No	Multiple instance learning + KNN, SVM	74	SE = 92.6%; SP = 88.1%
[3]	1	12	MI: 16,960 BE H: 3200 BE	Yes	Time domain features with DWT + KNN	36 (D,L)	SE = 99.97%; SP = 99.9% (D) SE = 98.67%; SP = 98.71% (L)
[9]	4	12	MI: 847 BE H: unknown	Yes	DWT multiscale energy eigenspace + SVM	72 (D,L)	ACC = 96%; SE = 93%; SP = 99% (D) ACC = 99.58% (L)
[10]	1	1	MI: 485,753 BE H: 125,652 BE	Yes	12 nonlinear features + KNN	47 (D) 25 (L)	ACC = 98.8%; SE = 99.45%; SP = 96.27% (D) ACC = 98.74%; SE = 99.55%; SP = 96.16% (L)
[5]	1	1	MI: 40,182 BE H: 10,546 BE	Yes	Deep convolutional neural network	_	ACC = 95.22%; SE = 95.49%; SP = 94.19%
[37]	1	1,12	MI: 485,752 BE H: 10,564 BE	Yes	Deep convolutional neural network	_	ACC = 99.78%
[7]	4	12	MI: 41,726 BE H: 9966 BE	No	DWT + High order singular value decomposition (HOSVD) + SVM	35 (D) 51 (L)	ACC = 95.3%; SE = 94.6%; SP = 96.0% (D) ACC = 98.1% (L)
Ourwork	1	12	MI: 47,215 BE H: 10,342 BE	No	Dual-Q TQWT + DWPT + MPCA + Treebagger	Record-level 84 (D,L) Beat-level 84 (D,L) 10 (D,L)	ACC = 97.46%; SE = 99.09%;SP = 90.26% (D) ACC = 90.39%; SE = 98.03%; SP = 90.76% (L) ACC = 99.98%; SE = 100%; SP = 99.9% (D) ACC = 99.87%; SE = 99.97%; SP = 99.88% (L) ACC = 99.41% (D); ACC = 99.35% (L)

D is MI detection, L is MI localization.

work is comparable to the earlier studies in the literature. We obtained an accuracy of 99.98% in MI detection and an accuracy of 99.87% in MI localization in beat level with 84 features. By using only 10 features in beat level, we obtained an accuracy of 99.41% in MI detection and an accuracy of 99.35% in MI localization. For the record level, we achieved an accuracy of 97.46% in MI detection and an accuracy of 90.39% in MI localization.

4.6. Computational complexity of methods

The proposed methods are implanted in MATLAB 2018b software in the Windows platform on a desk computer with Intel i5-7500 CPU (@ 3.4 GHz) and 8-GB RAM. For one record of ECG, the running time of Dual-Q TQWT (45.63 s) is shorter than the commonly used denoising algorithm EMD (225.89 s). The running time of DWPT feature extraction is 11.39 s, which is easier and more time-saving than features combination of linear, nonlinear, and entropy. Compared with the time spending on PCA (1795.21 s) used for dimensionality reduction, the tensor-based MPCA requires 123.84 s on 408 ECG records. The training and testing processes of Treebagger classifier spend 223.13 s and 0.67 s, respectively.

5. Conclusion

The power of machine learning and advanced signal processing provides an opportunity for intelligent medical assistance in clinical practice. However, automated, reliable, and real-time MI detection and localization is still a challenging problem because of artifacts corruption, high dimensionality, and inter-individual variations. In our present study, we introduced an automated MI detection and localization system using Dual-Q TQWT and wavelet packet tensor decomposition. By applying the Dual-Q TQWT denoising method, we achieved comparable good performance compared with the filtered data and commonly used denoising methods. Based on the low Q-factor component after denoising, a wavelet packet tensor was formed and then dimensionality reduced by tensor-based MPCA, which showed a better result than vector-based PCA. A total of 84 features chosen from MPCA dimensionality reduction were fed into a Treebagger classifier, reaching an accuracy of 97.46% in MI detection and an accuracy of 90.39% in MI localization considering the record variations. The high performance of our automated detection and localization system might be helpful in providing MI diagnosis care with minimal resources.

In future work, we will test the robustness of Dual-Q TQWT with different types of artifacts mixed with ECG data. Moreover, the automated MI detection and localization system will be applied to other heart disease diagnosis.

Declaration of Competing Interest

The authors have declared that no competing interests exist.

Acknowledgments

This work was supported by Fundamental Research Funds for the Central Universities in Dalian University of Technology in China (DUT2019, DUT16RC(3)021), the scholarships from China Scholarship Council (no. 201600090044, no. 201600090042), and the National Science Foundation of China (no. 91748105, no. 81471742, no. 61703069).

References

[1] K. Thygesen, J.S. Alpert, A.S. Jaffe, M.L. Simoons, B.R. Chaitman, H.D. White, Third universal definition of myocardial infarction, Circulation 126 (2012) 2020–2035, doi:10.1016/j.gheart.2012.08.001.

[2] B. Liu, J. Liu, G. Wang, K. Huang, F. Li, Y. Zheng, Y. Luo, F. Zhou, A novel electrocardiogram parameterization algorithm and its application in myocardial infarction detection, Comput. Biol. Med 61 (2015) 178–184, doi:10.1016/j.compbiomed.2014.08.010.

[3] M. Arif, I.A. Malagore, F.A. Afsar, Detection and localization of myocardial infarction using K-nearest neighbor classifier, J. Med. Syst. 36 (2012) 279–289, doi:10.1007/s10916-010-9474-3.

[4] R.J. Martis, U.R. Acharya, H. Adeli, Current methods in electrocardiogram characterization, Comput. Biol. Med. 48 (2014) 133–149, doi:10.1016/j.compbiomed.2014.02.012.

[5] Z. Chen, Emery N. Brown, R. Barbieri, Characterizing nonlinear heartbeat dynamics within a point process framework, IEEE Trans. Biomed. Eng 57 (2011) 1335–1347, doi:10.1109/TBME.2010.2041002.

[6] Y. Hagiwara, M. Adam, H. Fujita, J.H. Tan, S.L. Oh, U.R. Acharya, Application of deep convolutional neural network for automated detection of myocardial infarction using ECG signals, Inf. Sci. (Ny) 415–416 (2017) 190–198, doi:10.1016/j.ins.2017.06.027.

[7] L. Sun, Y. Lu, K. Yang, S. Li, ECG analysis using multiple instance learning for myocardial infarction detection, IEEE Trans. Biomed. Eng 59 (2012) 3348–3356, doi:10.1109/TBME.2012.2213597.

[8] S. Padhy, S. Dandapat, Third-order tensor based analysis of multilead ECG for classification of myocardial infarction, Biomed. Signal Process. Control 31 (2017) 71–78, doi:10.1016/j.bspc.2016.07.007.

[9] M. Kumar, R.B. Pachori, U.R. Acharya, Automated diagnosis of myocardial infarction ECG signals using sample entropy in flexible analytic wavelet transform framework, Entropy (2017) 19, doi:10.3390/e19090488.

[10] L.N. Sharma, R.K. Tripathy, S. Dandapat, Multiscale energy and eigenspace approach to detection and localization of myocardial infarction, IEEE Trans. Biomed. Eng. 62 (2015) 1827–1837, doi:10.1109/TBME.2015.2405134.

[11] U.R. Acharya, H. Fujita, V.K. Sudarshan, S.L. Oh, M. Adam, J.E.W. Koh, J.H. Tan, D.N. Ghista, R.J. Martis, C.K. Chua, C.K. Poo, R.S. Tan, Automated detection and localization of myocardial infarction using electrocardiogram: a comparative study of different leads, Knowledge-Based Syst. 99 (2016) 146–156, doi:10.1016/j.knosys.2016.01.040.

[12] Riccardo Barbieri, E.N. Brown, Analysis of heartbeat dynamics by point process adaptive filtering, IEEE Trans. Biomed. Eng. 53 (2006) 4–12, doi:10.1109/TBME.2005.859779.

[13] F.A. Elhaj, N. Salim, A.R. Harris, T.T. Swee, T. Ahmed, Arrhythmia recognition and classification using combined linear and nonlinear features of ECG signals, Comput. Methods Programs. Biomed. 127 (2016) 52–63, doi:10.1016/j.cmpb.2015.12.024.

[14] M. Blanco-Velasco, B. Weng, K.E. Barner, ECG signal denoising and baseline wander correction based on the empirical mode decomposition, Comput. Biol. Med. 38 (2008) 1–13, doi:10.1016/j.compbiomed.2007.06.003.

[15] R. Agarwal, J. Gotman, Computer-assisted sleep staging, IEEE Trans. Biomed. Eng. 48 (2001) 1412–1423, doi:10.1109/10.966600.

[16] I. Selesnick, in: TQWT, Toolbox Guide, NewYork, 2011, pp. 1–25.

[17] I.W. Selesnick, Wavelet transform with tunable Q-factor, IEEE Trans. Signal Process 59 (2011) 3560–3575, doi:10.1109/TSP.2011.2143711.

[18] I.W. Selesnick, Resonance-based signal decomposition: a new sparsity-enabled signal analysis method, Signal Processing 91 (2011) 2793–2809.

[19] R. Bousseljot, D. Kreiseler, A. Schnabel, Nutzung der EKG-Signaldatenbank Cardiodat der PTB über das internet, Biomed. Tech. 40 (1995) 317–318, doi:10.1515/bmte.1995.40.s1.317.

[20] S.H.Goldberger AL, L.A.N. Amaral, L. Glass, J.M. Hausdorff, Ivanov PCh, R.G. Mark, J.E. Mietus, G.B. Moody, C.-.K. Peng, PhysioBank, PhysioToolkit, and PhysioNet components of a new research resource for complex physiologic signals, Circulation 101 (2000) 215–220, doi:10.1161/01.CIR.101.23.e215.

[21] A. Delorme, S. Makeig, EEGLAB: an open source toolbox for analysis of single-trial EEG dynamics including independent component analysis, J. Neurosci. Methods 134 (2004) 9–21, doi:10.1016/j.jneumeth.2003.10.009.

[22] S.N. Yu, K.T. Chou, Integration of independent component analysis and neural networks for ECG beat classification, Expert Syst. Appl. 34 (2008) 2841–2846, doi:10.1016/j.eswa.2007.05.006.

[23] J.L. Starck, M. Elad, D.L. Donoho, Image decomposition via the combination of sparse representations and a variational approach, IEEE Trans. Image. Process. 14 (2005) 1570–1582, doi:10.1109/TIP.2005.852206.

[24] M.V. Afonso, J.M. Bioucas-Dias, M.A.T Figueiredo, Fast image recovery using variable splitting and constrained optimization, IEEE Trans. Image. Process. 19 (2010) 2345–2356, doi:10.1109/TIP.2010.2047910.

[25] A.R. Hassan, M.I.H. Bhuiyan, A decision support system for automatic sleep staging from EEG signals using tunable Q-factor wavelet transform and spectral features, J. Neurosci. Methods 271 (2016) 107–118, doi:10.1016/j.jneumeth.2016.07.012.

[26] S. Chaibi, T. Lajnef, Z. Sakka, M. Samet, A. Kachouri, A reliable approach to distinguish between transient with and without HFOs using TQWT and MCA, J. Neurosci. Methods 232 (2014) 36–46, doi:10.1016/j.jneumeth.2014.04.025.

[27] S. Patidar, R.B. Pachori, N. Garg, Automatic diagnosis of septal defects based on tunable-Q wavelet transform of cardiac sound signals, Expert Syst. Appl. 42 (2015) 3315–3326, doi:10.1016/j.eswa.2014.11.046.

[28] S. Patidar, R.B. Pachori, Classification of cardiac sound signals using constrained tunable-Q wavelet transform, Expert Syst. Appl. 41 (2014) 7161–7170, doi:10.1016/j.eswa.2014.05.052.

[29] S. Patidar, T. Panigrahi, Detection of epileptic seizure using Kraskov entropy applied on tunable-Q wavelet transform of EEG signals, Biomed. Signal Process. Control 34 (2017) 74–80, doi:10.1016/j.bspc.2017.01.001.

[30] J. Pan, W.J Tompkins, A real-time QRS detection algorithm, IEEE Trans. Biomed. Eng. BME-32 (1985) 230–236, doi:10.1109/TBME.1985.325532.
[31] H. He, Y. Tan, J. Xing, Unsupervised classification of 12-lead ECG signals using wavelet tensor decomposition and two-dimensional Gaussian spectral clustering, Knowledge-Based Syst. 163 (2019) 392–403, doi:10.1016/j.knosys.2018.09.001.
[32] H. Lu, K.N. Plataniotis, A.N. Venetsanopoulos, MPCA: multilinear principal component analysis of tensor objects, IEEE Trans. Neural Netw. 19 (2008) 18–39, doi:10.1109/TNN.2007.901277.
[33] H. Lu, K.N. Plataniotis, A.N. Venetsanopoulos, A survey of multilinear subspace learning, Pattern Recognit. 44 (2011) 1540–1551, doi:10.1016/j.physb.2011.12.087.
[34] J. Wang, A. Barreto, L. Wang, Y. Chen, N. Rishe, J. Andrian, M. Adjouadi, Multilinear principal component analysis for face recognition with fewer features, Neurocomputing 73 (2010) 1550–1555, doi:10.1016/j.neucom.2009.08.022.
[35] H. He, Y. Tan, Pattern clustering of hysteresis time series with multivalued mapping using tensor decomposition, IEEE Trans. Syst. Man Cybern. Syst. 48 (2018) 993–1004, doi:10.1109/TSMC.2017.2737578.
[36] B. Kamiński, M. Jakubczyk, P. Szufel, A framework for sensitivity analysis of decision trees, Cent. Eur. J. Oper. Res. 26 (2018) 135–159, doi:10.1007/s10100-017-0479-6.
[37] T.G. Dietterich, An experimental comparison of three methods for constructing ensembles of decision trees, Mach. Learn. 40 (2000) 139–157, doi:10.1023/A:1007607513941.
[38] D.G. Altman, J.M Bland, Diagnostic tests 1 - sensitivity and specificity, Med. Stat. Lab. Imp. Canser Res. Fund London 308 (1994) 1552, doi:10.1258/phleb.2012.012J05.
[39] D.M.W. Powers, Evaluation: from precision, recall and F-measure to ROC, informedness, markedness and corrrelation, J. Mach. Learn. Technol. 2 (2011) 37–63.
[40] U.B. Baloglu, M. Talo, O. Yildirim, R.S. Tan, U.R. Acharya, Classification of myocardial infarction with multi-lead ECG signals and deep CNN, Pattern Recognit. Lett. 122 (2019) 23–30, doi:10.1016/j.patrec.2019.02.016.
[41] H. Fujita, D. Cimr, Decision support system for arrhythmia prediction using convolutional neural network structure without preprocessing, Appl. Intell. (2019), doi:10.1007/s10489-019-01461-0.
[42] U.R. Acharya, H. Fujita, S.L. Oh, U. Raghavendra, J.H. Tan, M. Adam, A. Gertych, Y. Hagiwara, Automated identification of shockable and non-shockable life-threatening ventricular arrhythmias using convolutional neural network, Futur. Gener. Comput. Syst. 79 (2018) 952–959, doi:10.1016/j.future.2017.08.039.
[43] H. Fujita, D. Cimr, Computer aided detection for fibrillations and flutters using deep convolutional neural network, Inf. Sci. (Ny). 486 (2019) 231–239, doi:10.1016/j.ins.2019.02.065.